




Investigating the electronic and nonlinear optical properties of fullerene by substituting N, P, As, and Sb in the lattice structure: a DFT study

Samir Thakur¹ · Sankar M. Borah¹ · Ashok Singh² · Nirab C. Adhikary³ 

Received: 20 September 2019 / Accepted: 8 January 2020 / Published online: 27 January 2020
© Springer-Verlag GmbH Germany, part of Springer Nature 2020

Abstract

In this article, we used density functional theory (DFT) to investigate the structural, electronic and nonlinear optical properties of N, P, As and Sb doped fullerene. The average polarizability and hyperpolarizability is significantly improved when these impurities are substituted individually in the (C₆₀) lattice structure. The maximum hyperpolarizability is calculated for N-doped fullerene (3541.27 au) followed by P-doped fullerene (259.71 au), As-doped fullerene (102.52 au) and Sb-doped fullerene (32.06 au). A similar trend is observed and the polarizability is found to decrease monotonically. Both the polarizability and hyperpolarizability values are found to decrease with an increasing energy gap of the doped fullerene. N-Doped fullerene has the lowest energy gap (1.28 eV) followed by P-doped fullerene (1.94 eV), As-doped fullerene (2.02 eV) and Sb-doped fullerene (2.10 eV). The lowest energy gap minimizes the excitation energy and thus improves the nonlinear optical response. From the calculation of time-dependent-DFT (TD-DFT), it is observed that the maximum absorption wavelength of N-doped fullerene, which is about 830 nm, is shifted towards the longer wavelength at the infrared region in the case of P, As, and Sb-doped fullerenes. The results obtained through this study will help encourage the potential utilization of the metal-free doped-fullerene systems as a form of unique optical devices, thermal radiation detector, etc.

Keywords Fullerene · Density function theory · Partial density of states · Energy gap · Polarizability · Hyperpolarizability

1 Introduction

Through a previous couple of years, the design of new materials with remarkable non-linear optical (NLO) properties has gained significant attention due to their many applications in optoelectronics, photonic devices, bio-sensing, imaging, optical telecommunications, semiconductors,

second harmonic generation, etc. [1–8]. Materials, which can alter the fundamental parameters of an incident optical beam, such as phase, amplitude, frequency, etc., received tremendous attention for nonlinear optical activity (NLO). A variety of organic, inorganic, organometallic and polymer materials exist which show the NLO activity. A wide range of methods have already been discovered in the literature (such as electron push–pull mechanism, metal–organic assemblies) to further improve the NLO properties of various materials. Hyperpolarizability also increases due to excess diffuse electrons [9]. Alkali metal atoms have significant contribution to make the molecular structure electron rich system. These excessive electrons received from metals reduce the excitation energy and, therefore, increases the NLO response [10–13]. Substituting is one of the most efficient methods for altering the electronic properties of the structure to have a sufficient number of electrons and holes [14–18]. The literature shows numerous articles that review information about the excess electron approach employed to have large hyperpolarizability values [6–8]. For example, Niu et al. [6] observed the large first-order

Electronic supplementary material The online version of this article (<https://doi.org/10.1007/s00339-020-3300-7>) contains supplementary material, which is available to authorized users.

✉ Nirab C. Adhikary
nirab_iasst@yahoo.co.in

¹ Physical Science Division, Department of Applied Sciences, Gauhati University, Guwahati, Assam 781014, India

² Department of Physics, Science College, BTC, Kokrajhar, Assam 783370, India

³ Physical Sciences Division, Institute of Advanced Study in Science Technology, Paschim Boragaon, Garchuk, Guwahati, Assam 781035, India

hyperpolarizability in the $\text{Al}_{12}\text{N}_{12}$ nanocage fullerene-like structure by substituting Li, Na and K in the crystal lattice. In a second study, Maria et al. [7] described exactly how the substituting of the alkali metal atom influences the hyperpolarizability of BN nanocages. They found enhancement in the NLO properties and first-order hyperpolarizability right after metal incorporation. The hyperpolarizabilities associated with the doped structures vary from 103 to 105 au in comparison to 0 au for undoped structure.

Carbon and its allotropes are considered one among the rising fields of research in the twenty-first century with multi-disciplinary approaches. Rapid improvement of science and technology provides many advanced experimental methods such as chemical vapour deposition (CVD) [19], catalytic chemical vapour deposition (CCVD) [20], high vacuum chemical vapour deposition (HVCVD) [21], microwave plasma chemical vapour deposition (MWCVD), etc., are extensively used for synthesizing these materials [22]. In historical perspectives, Kroto first observed fullerenes in 1985 [23]. The discovery of fullerenes opened an era for the new synthetic molecular allotrope of carbon. Later on, the discovery of carbon nanotubes [24] and graphene [25] in 1991 and 2004, respectively, revealed the diverse structural, electronic and optical properties of these organic compounds for varieties of applications. C_{60} , considered to be the most stable carbon allotropes, consists of 60 sp^2 hybridized carbon atoms that are bonded in a spherical structure. Functionalization of fullerene is one of the most desired fields of research, which have been investigated both theoretically and experimentally by many researchers [26]. The intrinsic physical, chemical and optical properties of fullerene is significantly affected when heteroatoms are used as dopants to their lattice structures. Moreover, studies also show that fullerenes derivatives exhibit non-linear optical properties [27–29]. Apart from this, fullerenes and its derivatives with polymer composites are widely used as an active catalyst in electrochemical reactions, as well as in organic solar cells as an electron acceptor [30, 31]. Many researchers investigated the fundamental properties of fullerenes. Among all those researchers, Feng Gao et al. found that N-doped fullerene, as a catalyst, is suitable for hydrogen fuel cells [32]. Apart from that, research carried out by Fahimeh Hassani et al. reveals a strong non-covalent interaction in between sulphur doped fullerene and iodine molecules to use it in drug delivery application for hyperthyroidism treatment [33].

Due to the large surface area and spherical structure, the carbon atoms of the fullerene, experiences strain. Hence, it raises the internal energy in comparison with strain-free compound and strained carbon bonds provide a significant contribution to the polarizability of the structure. Therefore, it is important to study how the electronic polarization changes when different impurities are individually substituted in the fullerene lattice structure and its contribution

towards the enhancement of non-linear optical activity. The literature consists of full of articles in which electronic, and nonlinear optical properties of a system are significantly influenced by substituting [34–36]. Although limited reviews are found on how the non-metal donor impurities (for example N-Group elements) affect the NLO properties of fullerene, exohedral, endohedral and substitution are the three different ways in which impurities are added to fullerenes. However, in this article, we proceed with the substitution that involves the replacement of one carbon atom of fullerene with a dopant. The optimized structures of doped fullerenes, frontier highest occupied molecular orbital (HOMO) and lowest unoccupied molecular orbitals (LUMO) along with their energy gaps (E_g) and density of states (DOS) are calculated using DFT. Furthermore, natural bonding orbital analysis (NBO) and time-dependent-DFT simulations were carried out to investigate the partial charge distribution on the fullerene surface and also to find out the optical properties such as UV–visible absorption spectrum of the doped fullerenes. The polarizability tensor and first order hyper polarizability are also calculated to investigate the non-linear optical properties.

2 Computational details

The DFT implemented under Gaussian 09 software package [37] is used to simulate doped and undoped fullerene structures. Till date, numerous analyses have been done by many researchers as well as by our group using this theory in the field of material science [38–43]. In all calculations, Becke, three-parameter, Lee–Yang–Parr [B3LYP] exchange–correlation functional [44] along with 6–31 G (d) basis set is adapted for the pristine, N, P and As-doped fullerenes and Los Alamos National Laboratory 2 Double-Zeta (LANL2DZ) [45] basis set is used for optimizing the Sb -doped fullerene structures. Here, the LANL2DZ basis set is chosen because it offers an effective core potential (ECP), which considers relativistic effects for heavy atoms. In this case, core electrons represented by an ECP. Literature reveals that both 6-31G(d) + LANL2DZ mixed basis set significantly reduce the computational cost [46] and consider both light and heavy dopants during the optimization. This computational approach has been used previously by many researchers [47, 48]. The reason for choosing B3LYP hybrid functional is that it provides reasonable bond lengths and angles within 0.02 Å and 2°, respectively. Moreover, it does not underestimate HOMO–LUMO gaps and gives precise values of polarizabilities and hyperpolarizabilities for atomic as well as large molecular systems. Therefore, it is better suited for the study of non-linear optical property [49, 50]. Here, the buckyball structure of fullerene (C_{60}) is designed with 60 carbon atoms.

These structures are geometrically optimized in the gas phase without any symmetry constraint using restricted and unrestricted DFT and no imaginary frequencies are obtained, which represents that all the structures having minimum energy configuration. The optimized fullerene is then individually doped with N, P, As and Sb. The absorption wavelengths of optimized ground state structures are calculated by time-dependent-DFT at the B3LYP/6-31G (d) + LANL2DZ level. In addition, the other properties, such as molecular orbitals, natural population analysis (NPA), HOMO–LUMO energy gap, the DOS, electrostatic potentials and NBO are also obtained from the simulation. Gauss view and GaussSUM [51] programs are used for visualization and calculations of the total and partial DOS.

To study the stability of pure and doped fullerenes, chemical potential (μ), hardness (η), softness (S) and electrophilicity (ω) values are determined using the subsequent equations, respectively [52].

$$\mu = \frac{-(E_{\text{HOMO}} + E_{\text{LUMO}})}{2}, \tag{1}$$

$$\eta = \frac{E_{\text{LUMO}} - E_{\text{HOMO}}}{2\eta}, \tag{2}$$

$$S = \frac{1}{2\eta}, \tag{3}$$

$$\omega = \frac{\mu^2}{2\eta}. \tag{4}$$

In the above equation, E_{HOMO} and E_{LUMO} represent the energies of HOMO and LUMO respectively. Polarizability (α) and hyperpolarizability (β) develop when a uniform electric field is applied to a molecular system. Taylor expansion is used to write the energy of a system (E) in accordance with a uniform external electric field (F) [53].

$$\begin{aligned} E(F) &= E(0) + \left. \frac{\partial E}{\partial F} \right|_{F=0} F + \frac{1}{2} \left. \frac{\partial^2 E}{\partial F^2} \right|_{F=0} F^2 + \frac{1}{6} \left. \frac{\partial^3 E}{\partial F^3} \right|_{F=0} F^3 + \frac{1}{24} \left. \frac{\partial^4 E}{\partial F^4} \right|_{F=0} F^4 + \dots \\ &= E(0) - \mu F - \frac{1}{2} \alpha F^2 - \frac{1}{6} \beta F^3 - \frac{1}{24} \gamma F^4 \\ \mu &= - \left. \frac{\partial E}{\partial F} \right|_{F=0}; \quad \alpha = - \left. \frac{\partial^2 E}{\partial F^2} \right|_{F=0}; \quad \beta = - \left. \frac{\partial^3 E}{\partial F^3} \right|_{F=0}; \quad \gamma = - \left. \frac{\partial^4 E}{\partial F^4} \right|_{F=0}, \end{aligned}$$

where the vector μ is the permanent dipole moment and is a second rank tensor; β is called the first-order hyperpolarizability, which is a third rank tensor and known as second-order nonlinear optical response coefficient; γ is known as the second-order hyperpolarizability, which is a fourth rank

tensor and called as third-order NLO coefficient. However, the calculation of second-order hyperpolarizability is computationally expensive, therefore in this calculation, we centred our study limited up to the first-order hyperpolarizability only. One can predict whether the material will show NLO characteristics based on the first-order hyperpolarizability. NLO behaviour is expected to be shown in molecules with larger hyperpolarizability values. In the following equations, the average isotropic polarizability (a) and total first-order hyperpolarizability (β_0) are described as [7].

$$\langle \alpha \rangle = \frac{1}{3}(\alpha_{xx} + \alpha_{yy} + \alpha_{zz}) \tag{5}$$

$$\begin{aligned} \beta_0 &= [(\beta_{xxx} + \beta_{yyy} + \beta_{zzz})^2 + (\beta_{yyy} + \beta_{yzz} + \beta_{yxx})^2 \\ &\quad + (\beta_{zzz} + \beta_{zxx} + \beta_{zyy})^2]^{1/2}, \end{aligned} \tag{6}$$

where α_{xx} , α_{yy} , α_{zz} and β_{xxx} , β_{yyy} , etc. are the elements of the second rank polarizability tensor and third rank hyperpolarizability tensor respectively in different directions. So far as the DOS are concerned, it describes the number of states per unit volume available for the charges to occupy each energy. It is used to describe the localized states distributed in a given energy range. In some publications, exponential distribution is assumed while representing the DOS spectrum in case of semiconductors [54].

$$g(E) = \frac{N}{k_B T_0} \exp\left(\frac{-E}{k_B T_0}\right),$$

where N is the total DOS and T_0 is the parameter which indicates the width of the exponential distribution. However, some other publications, Bäessler et al. used a Gaussian shape of the DOS to describe the distribution of localized states described by the energetically disorder parameter σ_{DOS} and E_i which is the central energy of the HOMO or LUMO, the expression is

$$g(E) = \frac{N}{\sqrt{2\pi}\sigma_{\text{DOS}}} \exp\left(-\frac{(E - E_i)^2}{2\sigma_{\text{DOS}}^2}\right).$$

Several researchers worked regarding the impact of the DOS shape on the electronic properties of semiconductors

using simulations and experiments and discovered that a gaussian shape of the DOS most likely provides a reasonable explanation [55].

3 Results and discussion

3.1 Optimized structures

Initially, a model of pristine fullerene is designed and the geometrically optimized final structure is shown in Fig. 1. Now to get the most favourable doped fullerene structures, a substituting site is selected and denoted by X on the carbon surface (Fig. 1a). After that, N is doped by replacing the carbon atom belongs to the substituting site Fig. 1b and then the structure is allowed to re-optimize. Further, P, As and Sb atoms are individually doped and the re-optimized structures are shown in Fig. 1c–e. It is clear from the figures that, structural deformations occur on the fullerene surface when it is individually doped with N, P, As and Sb atoms. The C–C bond length of the pristine fullerene is found to be (~ 1.45 Å). However, in case of N, P, As and Sb-doped fullerenes the individual bond-lengths of the dopant atom and surrounding carbon atom are found to be 1.42 Å, 1.84 Å, 1.94 Å and 2.12 Å, respectively (Table 1). Therefore, an average increase of bond length observed in these doped structures. The calculated bond angle of $\angle C1-N-C2$, in N doped fullerene is found to be 107° and for $\angle C1-P-C2$, $\angle C1-As-C2$ and $\angle C1-Sb-C2$ is found to be 97.240, 92.740 and 86.250, respectively (Table 2), which is less in comparison to the bond angle of carbon atoms on the surface of the pristine fullerene. Due to the variation of bond-lengths and bond angles, the position of the dopant atoms in the

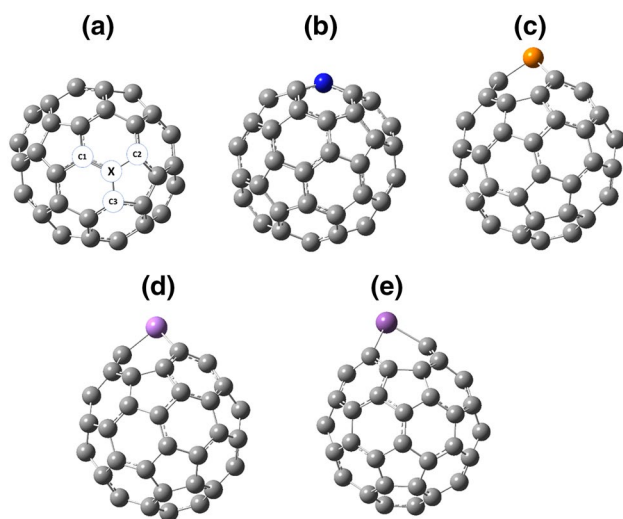


Fig. 1 The optimized structures of **a** pristine fullerene, **b** N doped fullerene, **c** P doped fullerene, **d** As doped fullerene, **e** Sb doped fullerene

Table 1 The bond length of pristine and doped fullerenes in Å

	C1-X	C2-X	C3-X
Pristine	1.45	1.45	1.45
N doped fullerene	1.42	1.42	1.40
P doped fullerene	1.80	1.84	1.84
As doped fullerene	1.91	1.94	1.94
Sb doped fullerene	2.15	2.12	2.15

optimized geometries is shifted to upward and creates a structural distortion on the carbon surface. The local bonding environment of fullerene is significantly affected by the addition of these dopants due to the variation of their covalent radii (0.76 Å, 0.71 Å, 1.07 Å, 1.19 Å and 1.39 Å for C, N, P, As and Sb, respectively) [56] and electro-negativities (2.55, 3.04, 2.19, 2.18 and 2.05 for C, N, P, As and Sb, respectively) [57].

3.2 Natural bonding orbital analysis

NBO is used to examine the delocalization of the electron density, hyperconjugation effects and several second-order interactions in the molecular system. Many authors used this method to analyse interaction energies. Among those authors, Maryam Koohi and co-workers found the intermolecular charge transfer from donor to the acceptor in substituted heterofullerenes. Their study reveals that the stability of heterofullerene increases with higher second-order perturbation interaction [58]. In this study, the nature of the bonding orbitals of individual dopant and nearby carbon atoms are shown in Table 3. In the case of N, and P substituted fullerene, the occupancy of the bonding orbitals varies from 0.98805 to 0.98951 and from 0.97615 to 0.97793, respectively. However, for the As and Sb substituted fullerene, it is found that the occupancy of the bonding orbitals varies from 0.97455 to 0.97597 and from 0.97667 to 0.96675, respectively.

3.3 Natural population analysis

NPA is performed based on the NBO, which is implemented under the Gaussian09 package. The distribution of the

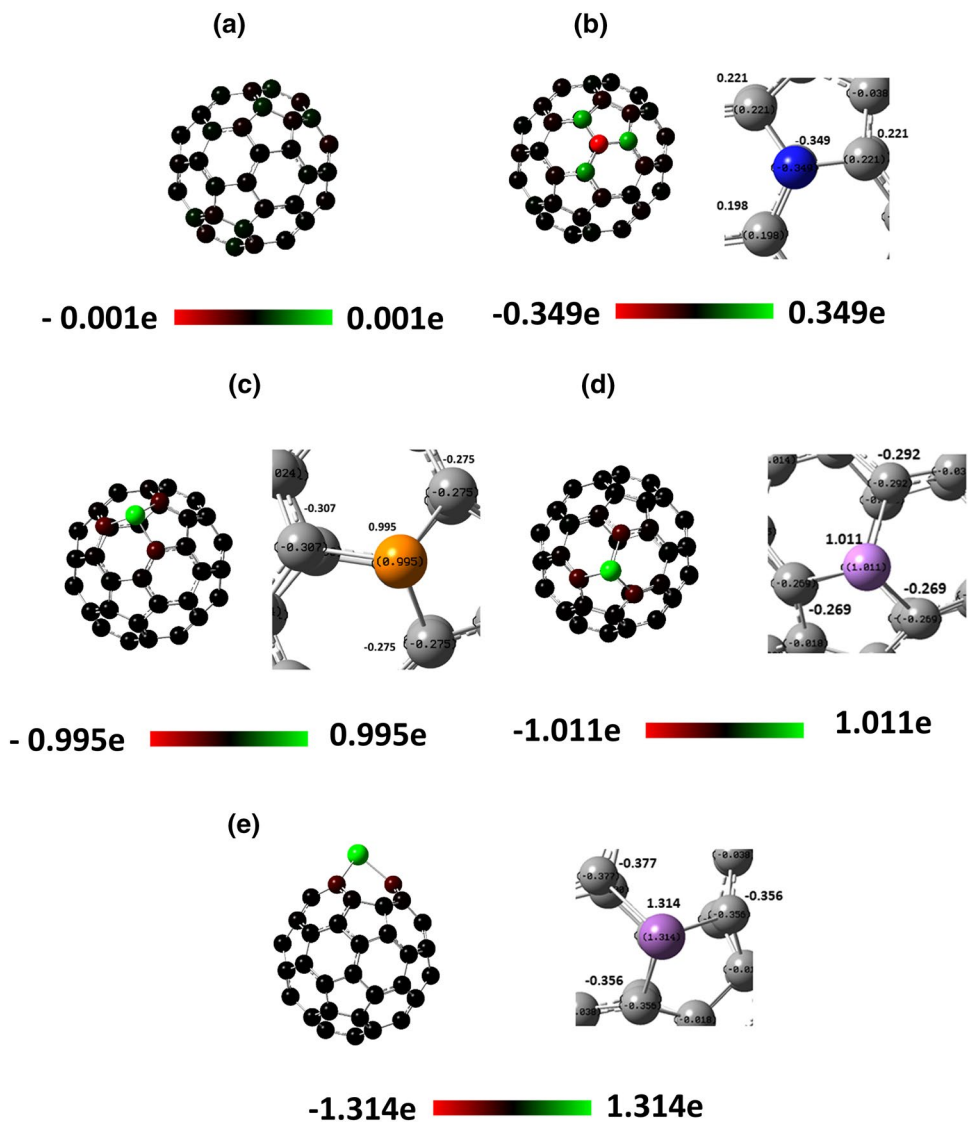
Table 2 The bond angles of pristine and doped fullerenes

	$\angle C1-X-C2$	$\angle C2-X-C3$	$\angle C3-X-C1$
Pristine	120°	120°	108°
N doped fullerene	107°	118.80°	118.79°
P doped fullerene	97.24°	97.24°	87.93°
As doped fullerene	92.74°	83.34°	92.74°
Sb doped fullerene	86.25°	77.34°	86.25°

Table 3 Natural bonding orbital analysis

System	Bonding orbital	Occupancy	Composition
N-substituted fullerene	C1-N	0.98806	37.19% C1 $sp^{2.82}$ + 62.81% N $sp^{2.23}$
	C2-N	0.98951	37.23% C2 $sp^{2.53}$ + 62.77% N $sp^{2.02}$
	C3-N	0.98805	37.19% C3 $sp^{2.82}$ + 62.81% N $sp^{2.23}$
P-substituted fullerene	C1-P	0.97615	64.80% C1 $sp^{2.70}$ + 35.20% P $sp^{5.62}$
	C2-P	0.97615	64.80% C2 $sp^{2.70}$ + 35.20% P $sp^{5.62}$
	C3-P	0.97793	65.38% C3 $sp^{2.23}$ + 34.62% P $sp^{5.01}$
As-substituted fullerene	C1-As	0.97455	65.83% C1 $sp^{2.91}$ + 34.17% As $sp^{7.74}$
	C2-As	0.97455	65.83% C2 $sp^{2.91}$ + 34.17% As $sp^{7.74}$
	C3-As	0.97597	66.70% C2 $sp^{2.38}$ + 33.30% As $sp^{6.97}$
Sb-substituted fullerene	C1-Sb	0.96675	70.51% C1 $sp^{3.32}$ + 29.49% Sb $sp^{9.89}$
	C2-Sb	0.96675	70.51% C2 $sp^{2.58}$ + 29.49% Sb $sp^{9.89}$
	C3-Sb	0.97667	71.00% C2 $sp^{2.58}$ + 29.00% Sb $sp^{8.92}$

Fig. 2 The total charge distribution of NBO analysis (in unit of electrons) of **a** pristine fullerene, **b** N doped fullerene, **c** P doped fullerene, **d** As doped fullerene and **e** Sb doped fullerene



partial charges of doped and undoped fullerene structures are shown in terms of the charge of the electron and with a scaled colour bar at the bottom of each Fig. 2. The red, black and green indicate the negative, neutral and positive charges, respectively on the fullerene surface. The result obtained from NPA signifies that the surface of the pristine fullerene (Fig. 2a) is found to be neutral compared to the doped fullerenes. However, a significant change in the partial charge distribution is observed in the case of N, P, As and Sb -doped fullerenes. Due to the highest electronegativity, N is found to be negative ($-0.349e$) and its surrounding three carbon atoms are positively charged ($0.221e$, $0.221e$ and $0.198e$, respectively). Further, the partial charges of the neighbouring carbon atoms ($-0.377e$, $-0.356e$ and $-0.356e$) of Sb-doped fullerenes is higher compared to that of P doped ($-0.307e$, $-0.275e$, $-0.275e$) and As-doped ($-0.269e$, -0.269 , $-0.292e$) fullerenes. As far as the dopants are concern, Sb ($1.314e$) is found to be more positive than compared to P ($0.995e$) and As ($1.011e$).

3.4 Molecular orbital analysis

The distribution of the molecular orbitals is shown in Fig. 3. In case of pristine and N-doped fullerene, computed HOMO and LUMO are found to be localised on the carbon atoms of the pristine, N and the neighbouring carbon atoms as shown by Fig. 3a, b. The alpha HOMO is found to be localised on P, As, and Sb atoms, respectively, in P, As, and Sb-doped fullerenes (Fig. 3c–e). Moreover, it is observed that the alpha LUMO is delocalised on these substituting elements but localised on the surface carbon atoms. Results obtained from the present calculation of energy reveals that HOMO–LUMO energy gap (as shown in Fig. 4) of pristine fullerene (about 2.76 eV) decreases to 1.28 eV on N substituting. However, P, As and Sb substituting increases the energy gap and the overall increasing order followed by the dopant is N-fullerene < P-fullerene < As-fullerene < Sb-fullerene. Variation of E_g performs an important role to cause a remarkable change in the electrical conductivity. The relation between conductivity as well as energy gap is given by the equation $\sigma \propto \exp(-E_g/kT)$, where σ and k are defined as the conductivity and Boltzmann constant, respectively. From

Fig. 3 The molecular orbitals of HOMO and LUMO for **a** pristine fullerene and alpha HOMO and LUMO for **b** N doped fullerene, **c** P doped fullerene, **d** As doped fullerene and **e** Sb doped fullerene

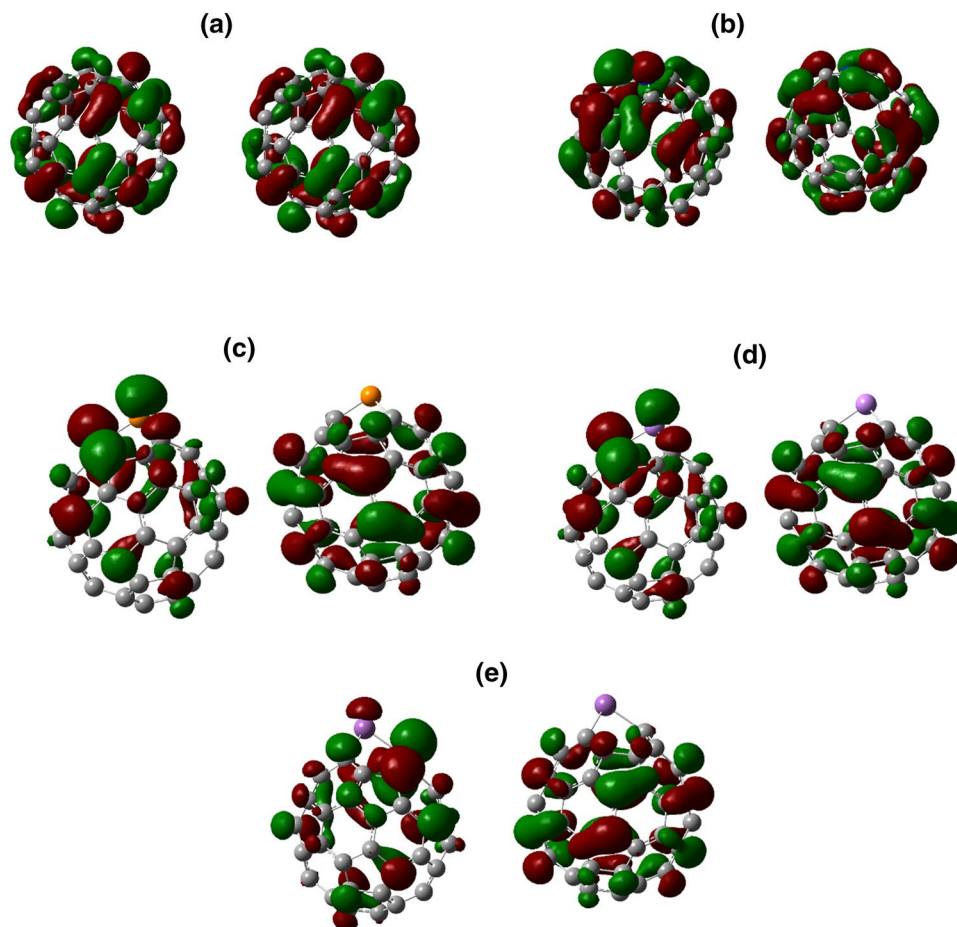
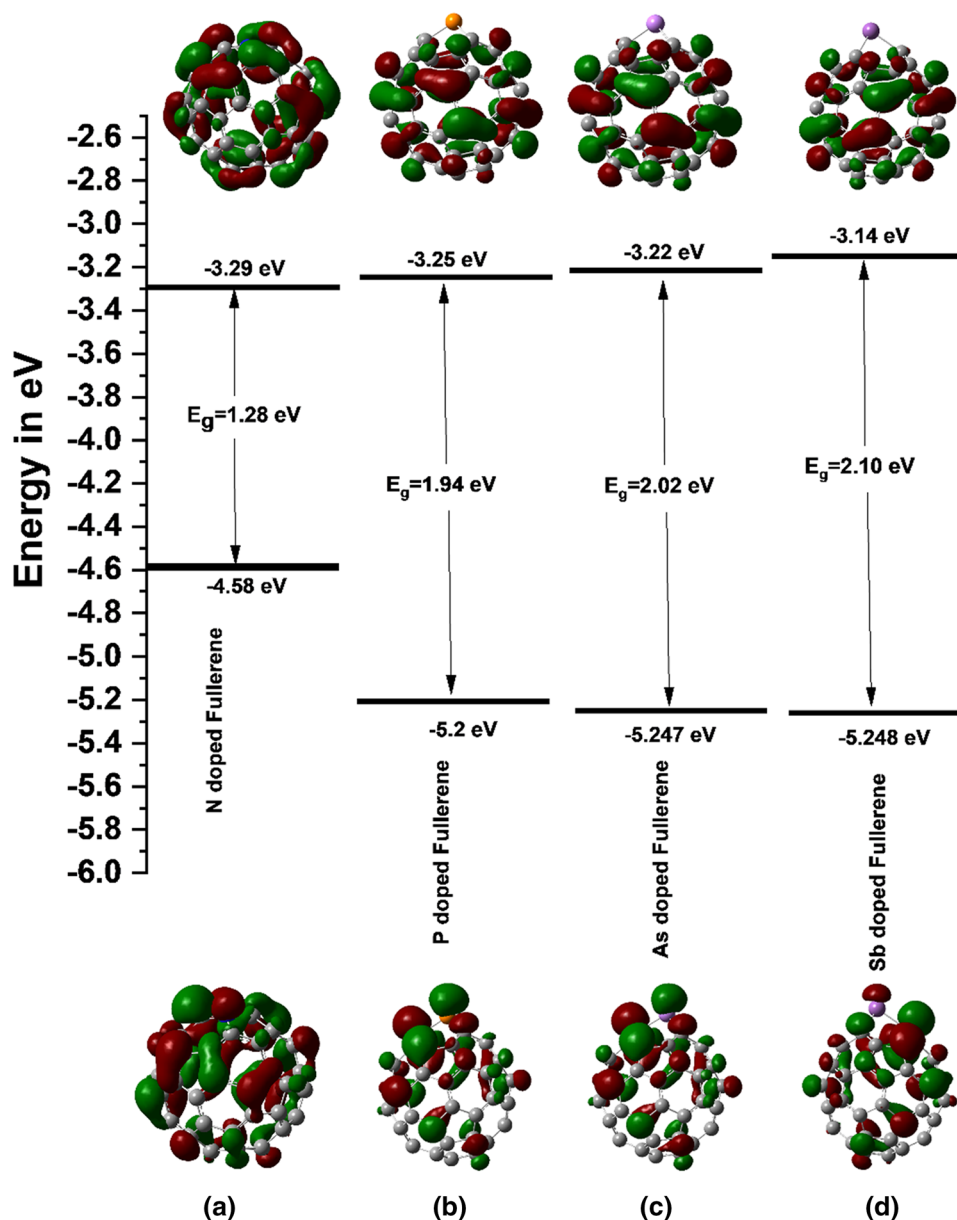


Fig. 4 Energy level diagram along with the molecular orbitals of **a** N-doped fullerene, **b** P-doped fullerene, **c** As-doped fullerene and **d** Sb-doped fullerene



the equation, it is usually seen that the small decrease in E_g causes considerably greater electrical conductivities [59].

3.5 DOS analysis

The DOS spectrum of undoped and doped fullerene structures is shown in Fig. 5. In the case of undoped fullerene, the Fermi energy level coincides with the HOMO energy level and it is found to be at -5.98 eV (Fig. 5a). Considering the alpha electron distribution, as we introduce different substituting element the Fermi energy level shifted from its original position. For N and As-doped fullerenes, it is observed that the partial DOS (PDOS) spectrum of N and As is overlapped with that of carbon at the Fermi energy

level, as shown by Fig. 5b, d, respectively. This overlapping signifies a strong orbital interaction of N and As to its neighbouring carbon atoms on the fullerene surface and Fermi level shifted to -4.58 eV and -5.24 eV for N and As-doped fullerene, respectively. Further, for Sb-doped fullerene in Fig. 5e the Fermi energy is found to be overlapped with HOMO energy. However, no significant orbital overlapping found in between the dopant and the carbon atoms at the Fermi level. The Fermi energy shifted to -5.24 eV. As far as P-doped fullerene is concerned, the Fermi energy shifted closer to LUMO at the higher energy (Fig. 5c).

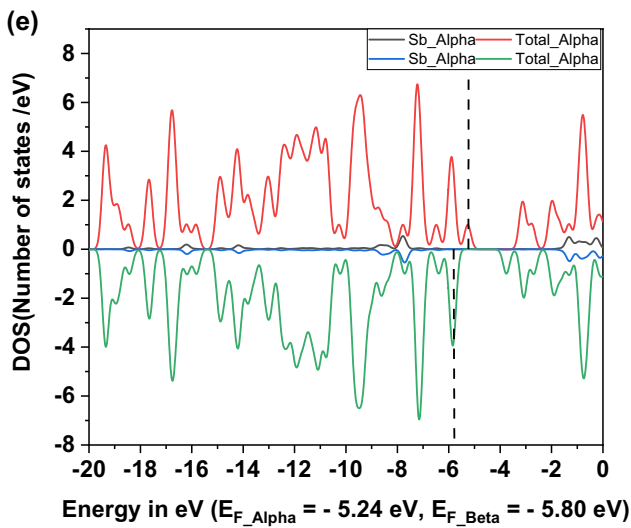
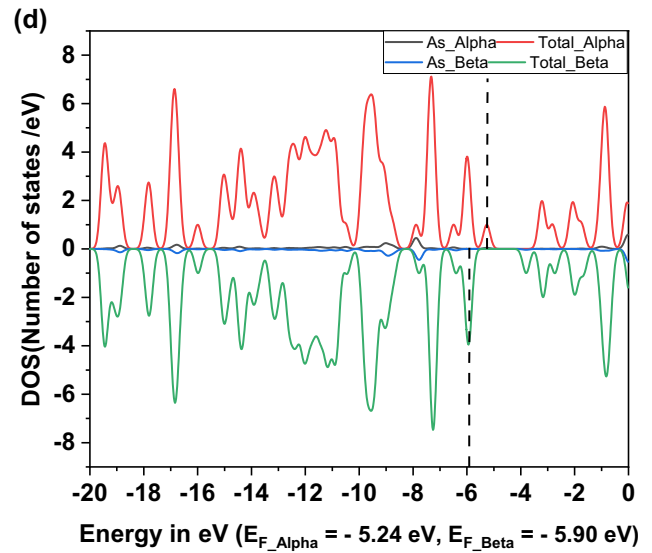
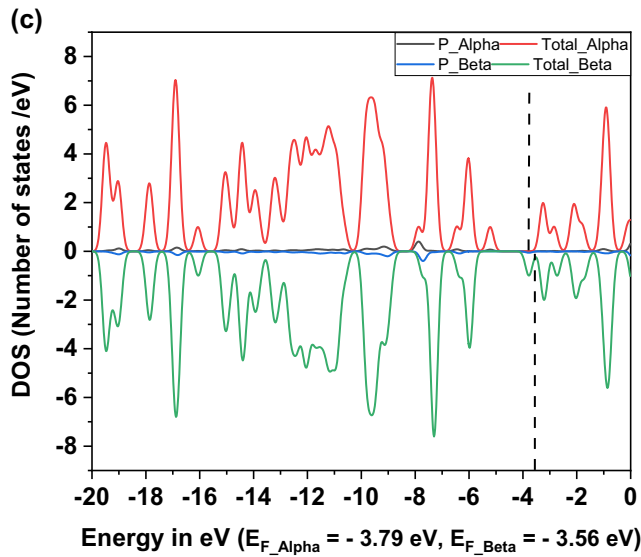
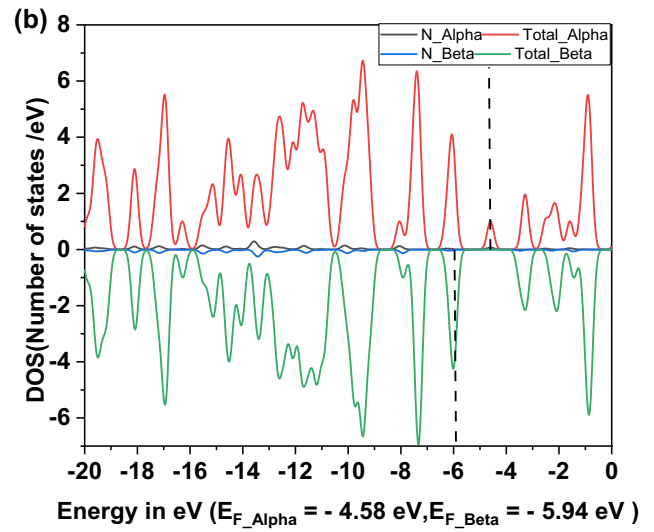
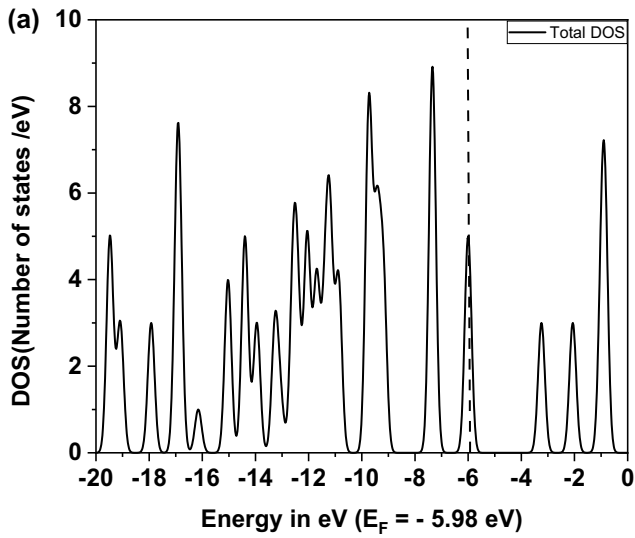


Fig. 5 **a** Total and partial density of states of pristine fullerene. **b** Total and partial density of states of N doped fullerene. **c** Total and partial density of states of P doped fullerene. **d** Total and partial density of states of As doped fullerene. **e** Total and partial density of states of Sb doped fullerene

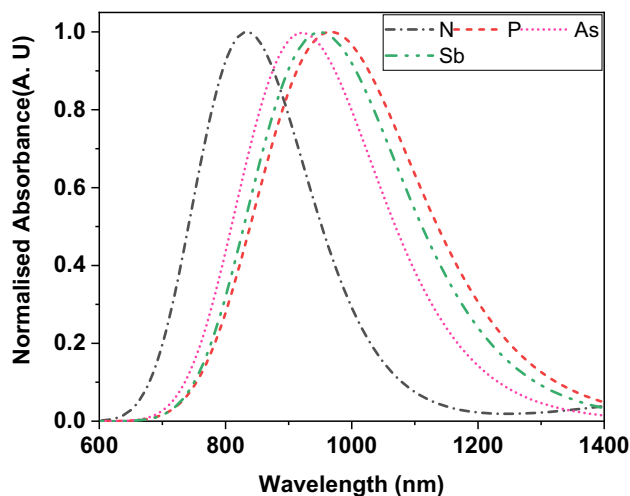


Fig. 6 UV-vis absorption spectra of N, P, As and Sb-doped fullerene as indicated by dash dot, dash, dot, and dash dot dot respectively

3.6 UV-vis absorption spectra

UV-vis absorption spectra as shown in Fig. 6 are computed using time-dependent-DFT (TD-DFT). Results obtained from the simulated spectrum signify that the absorption wavelength (λ) for N-doped fullerene is found to be at 830 nm. However, when the fullerene is doped with P, As and Sb atoms, the wavelength is shifted to the higher wavelength region. As far as P and As-doped fullerene are concerned, the wavelength is obtained at 967 nm and 922 nm, respectively. Further, in comparison to this, Sb-doped fullerene is found to absorb the wavelength at 954 nm.

3.7 Non-linear optical (NLO) properties

Analysis of hyperpolarizability provides significant information to understand the non-linear optical property of doped fullerenes. Polarizability and first-order static hyperpolarizability are calculated using sum over states (SOS) method under Multiwfn program [53, 60]. The output file generated by the Gaussian09 software is used as an input for the calculation of polarizability. Moreover, time-dependent DFT calculation is used to get the excited state energies and transition dipole moments for the SOS method. However, the result obtained from the calculations contains a large amount of data in the form of hyperpolarizability tensor. Therefore, we only discussed the dominant components,

which has important physical significance. In this case, all the units are converted to esu. As shown in Table 4, polarizabilities and hyperpolarizability values are found to be decreased significantly due to the increasing energy gap. As far as the N-doped fullerene (N-59) is concerned, the value of first-order static hyperpolarizability is found to be the highest (3541.27 au) followed by P-C59 (259.71 au), As-C59 (102.52 au) and Sb-C59 (32.06 au).

3.8 Quantum molecular descriptors

To find the stability and reactivity, we study the chemical potential (μ), hardness (η), softness (S), and electrophilicity (ω) of the doped and undoped fullerenes. The variation of molecular descriptors, which typically characterize specific information about the undoped and doped fullerene molecule, are presented Table 5. The hardness of fullerene decreases from 1.38 to 0.645 eV when it is doped with N. However, its value increases from P-doped to As-doped fullerene. The hardness of P and As doped fullerene is found to be 0.975 eV and 1.12 eV, respectively. For Sb-doped fullerene, the hardness is found to be 1.05 eV. Since hardness is a way of measuring stability for the chemical system against deformation; as a consequence, C60 is most stable, while C59-N and C59-P tend to be more prone to change under external deformation. As far as the softness is concerned, it is following the opposite trend to hardness. C59-N is the softest material with a softness value of 0.775 eV. Undoped fullerene is found to be the least soft with softness value 0.362 eV. The softness of P and As doped fullerene is 0.512 eV and 0.444 eV, respectively. Investigation of electrophilicity data indicates that the electrophilicity of C59-N is found to be the highest than comparing to undoped and other doped fullerenes. The electrophilicity of C59-P is 9.04 eV that reduces to 8.21 eV for C59-As and 8 eV for C59-Sb. However, undoped C60 has the lowest electrophilicity which is around 7.6 eV. The chemical potential of C60 is very close to C59-As, it shifts from -4.6 eV for C60 to -4.2 eV for C59-P and -4.1 eV for C59-Sb. The maximum change in chemical potential is noticed for C59-N.

4 Conclusion

DFT is used to study the substituting effect on the change in structural, electronic and nonlinear optical properties of doped fullerene. Here, the most stable spin states are undertaken throughout the optimization of individual doped fullerenes. It turns out that the energy gap of C60 fullerene keeps on increasing for all doped systems when moving from top to bottom in Group 15 (from N to Sb) of the periodic table. N-doped fullerene is found to have

Table 4 The non-linear polarizability and hyperpolarizabilities of doped fullerenes

System	Dipole moment (Debye)	Dipole moment (esu cm) ($\times 10^{-18}$)	Isotropic average polarizability (α) in atomic units (a.u.)	Isotropic average polarizability (α) in electronic units (esu) ($\times 10^{-24}$)	First order static hyper polarizability (β) in atomic units (a.u.)	First order static hyper polarizability (β) in electronic units (esu) ($\times 10^{-30}$)
N doped fullerene	1.22	1.22	11.47	1.69	3541.27	30.55
P doped fullerene	0.1346	0.13	2.6	0.385	259.71	2.24
As doped fullerene	0.5686	0.56	2.3	0.340	102.52	0.884
Sb doped fullerene	1.9372	1.93	2.03	0.30	32.06	0.276

Units of μ is in Debye (D), 1 Debye (D) = 1×10^{-18} esu cm, for α , 1 a.u. = 0.1482×10^{-24} esu, for β , 1 a.u. = 0.008629×10^{-30} esu [54]

Table 5 HOMO (H), LUMO (L), chemical potential (μ), hardness (η), softness (S), and electrophilicity (ω) of all system of undoped and doped fullerenes

System	HOMO (eV)	LUMO (eV)	μ (eV)	η (eV)	S (eV $^{-1}$)	ω (eV)
C60	- 5.98	- 3.22	- 4.6	1.38	0.362	7.6
C59-N	- 4.58	- 3.29	- 3.9	0.645	0.775	11.79
C59-P	- 5.2	- 3.25	- 4.2	0.975	0.512	9.04
C59-As	- 5.47	- 3.22	- 4.3	1.125	0.444	8.21
C59-Sb	- 5.24	- 3.14	- 4.1	1.05	0.476	8

the lowest energy gap and having the lowest LUMO energy level. The lowest energy gap signifies the highest conductivity compared to undoped and doped fullerenes. Moreover, our findings show that NPA charge on N doped fullerene is found negative. However, its strength is found positive which increases from P to Sb and the fullerene portion within these structures acquire a negative charge. The strength of negative charges is proportional to the magnitude of the positive charge on the non-metal. The polarizability of C60 increases when doped with non-metals. The highest level of polarizability and hyperpolarizability are estimated for N-doped fullerene which decreased progressively while moving from top to bottom in the group. The reduction in hyperpolarizability is due to the increase in the energy gap in that group. The higher energy gap increases the excitation energy and thus lowering the NLO response. The highest value of first-order hyperpolarizability in case of N-doped fullerene indicates that it is promising material showing non-linear optical properties. Moreover, the present investigation provides a significant contribution to study the enhancement of the conductivity of fullerene by tuning the energy gap in the presence of different substituting elements.

Acknowledgements The author would like to extend his sincere appreciation to the Physical Sciences Division, Institute of Advanced Study in Science and Technology (An Autonomous Institute under DST Govt. of India) and Department of Applied Sciences, Gauhati University for providing the computing facility for the simulation and their generous support. The author would also like to acknowledge the Director of Gauhati University Institute of Science and Technology, head, Dept. of Applied Sciences, Gauhati University and MHRD, Govt. of India, for offering Research Assistantship under TEQIP-III Project.

References

1. S. Muhammad, T. Minami, H. Fukui, K. Yoneda, R. Kishi, Y. Shigeta, M. Nakano, *J. Phys. Chem. A* **116**, 1417 (2012)
2. S. Muhammad, S. Ito, M. Nakano, R. Kishi, K. Yoneda, Y. Kitagawa, M. Shkir, A. Irfan, A.R. Chaudhry, S. AlFaify, A. Kalam, A.G. Al-Sehemi, *Phys. Chem. Chem. Phys.* **17**, 5805 (2015)
3. B. Champagne, A. Plaquet, J.L. Pozzo, V. Rodriguez, F. Castet, *J. Am. Chem. Soc.* **134**, 8101 (2012)
4. S. Muhammad, H.L. Xu, R.L. Zhong, Z.M. Su, A.G. Al-Sehemi, A. Irfan, *J. Mater. Chem. C* **1**, 5439 (2013)
5. S. Muhammad, H. Xu, Y. Liao, Y. Kan, Z. Su, *J. Am. Chem. Soc.* **131**, 11833 (2009)
6. M. Niu, G. Yu, G. Yang, W. Chen, X. Zhao, X. Huang, *Inorg. Chem.* **53**, 349 (2013)
7. J. Maria, K. Ayub Iqbal, *J. Alloys Compd.* **687**, 976 (2016)
8. M. Maria, J. Iqbal, K. Ayub, *RSC Adv.* **6**, 94228 (2016)
9. R.L. Zhong, H.L. Xu, Z.R. Li, Z.M. Su, *J. Phys. Chem. Lett.* **6**, 612 (2015)
10. W. Chen, Z.R. Li, D. Wu, Y. Li, R.Y. Li, C.C. Sun, *J. Phys. Chem. A* **109**, 2920 (2005)
11. F.F. Wang, Z.R. Li, D. Wu, B.Q. Wang, Y. Li, Z.J. Li, W. Chen, G.T. Yu, F.L. Gu, Y. Aoki, *J. Phys. Chem. B* **112**, 1090 (2008)
12. W. Chen, Z.R. Li, D. Wu, F.L. Gu, X.Y. Hao, B.Q. Wang, R.J. Li, C.C. Sun, *J. Chem. Phys.* **121**, 10489 (2004)
13. Z.J. Li, F.F. Wang, Z.R. Li, H.L. Xu, X.R. Huang, D. Wu, W. Chen, G.T. Yu, F.L. Gu, Y. Aoki, *Phys. Chem. Chem. Phys.* **11**, 402 (2009)
14. A.S. Rad, S.A. Aghouzi, N. Motaghedi, S. Maleki, M. Peyravi, *Mol. Simul.* **42**, 1519 (2016)
15. A.S. Rad, K. Ayub, *Comput. Theor. Chem.* **1138**, 39 (2018)
16. A.S. Rad, H. Pazoki, S. Mohseni, D. Zareyee, M. Peyravi, *Mater. Chem. Phys.* **182**, 32 (2016)
17. A.S. Rad, *J. Theor. Appl. Phys.* **10**, 307 (2016)
18. A.S. Rad, S.M. Aghaei, *Curr. Appl. Phys.* **18**, 133 (2018)
19. M.I. Ionescu, Y. Zhang, R. Li, H.A. Rachid, X. Sun, *Appl. Surf. Sci.* **258**, 4563 (2012)
20. G.N. Ilinich, B.L. Moroz, N.A. Rudina, I.P. Prosvirin, V.I. Bukhtiyarov, *Carbon* **50**, 1186 (2012)

21. F.H. Monteiro, D.G. Larrude, M.E.H. Maia da Costa, L.A. Terrazos, R.B. Capaz, F.L. Freire Jr., *J. Phys. Chem. C* **116**, 3281 (2012)
22. T. Watanabe, S. Tsuda, T. Yamaguchi, Y. Takano, *Physica C* **470**, S608 (2010)
23. H.W. Kroto, J.R. Heath, S.C. O'Brien, R.F. Curl, R.E. Smalley, *Nature* **318**, 162 (1985)
24. S. Iijima, *Nature* **354**, 56 (1991)
25. K.S. Novoselov, *Science* **306**, 666 (2004)
26. C. Tian, Z. Wang, M. Jin, W. Zhao, Y. Meng, F. Wang, W. Feng, H. Liu, D. Ding, D. Wu, *Chem. Phys. Lett.* **511**, 393 (2011)
27. Y. Wang, L.T. Cheng, *J. Phys. Chem.* **96**, 1530 (1992)
28. Z.B. Liu, Y.F. Xu, X.Y. Zhang, X.L. Zhang, Y.S. Chen, J.G. Tian, *J. Phys. Chem. B.* **113**, 9681 (2009)
29. Y.P. Sun, G.E. Lawson, J.E. Riggs, B. Ma, N. Wang, D.K. Moton, *J. Phys. Chem. A* **102**, 5520 (1998)
30. S.H. Noh, C. Kwon, J. Hwang, T. Ohsaka, B.J. Kim, T.Y. Kim, Y.G. Yoon, Z. Chen, M.H. Seo, B. Han, *Nanoscale* **9**, 7373 (2017)
31. B.C. Thompson, J.M.J. Fréchet, *Angew. Chem. Int. Ed.* **47**, 58 (2008)
32. F. Gao, G.L. Zhao, S. Yang, J.J. Spivey, *J. Am. Chem. Soc.* **135**, 3315 (2013)
33. F. Hassani, H. Tavakol, *Sens. Actuators B Chem.* **196**, 624 (2014)
34. M. Kurban, *Optik* **172**, 295 (2018)
35. I. Muz, M. Kurban, *J. Alloys Compd.* **802**, 25 (2019)
36. I. Muz, M. Kurban, K. Snli, *Inorg. Chim. Acta* **474**, 66 (2018)
37. M. J. Frisch, G. W. Trucks, H.B. Schlegel, G.E. Scuseria, M.A. Robb, J.R. Cheeseman, G. Scalmani, V. Barone, B. Men-nucci, G.A. Petersson, H. Nakatsuji, M. Caricato, X. Li, H.P. Hratchian, A.F. Izmaylov, J. Bloino, G. Zheng, J.L. Sonnenberg, M. Hada, M. Ehara, K. Toyota, R. Fukuda, J. Hasegawa, M. Ishida, T. Nakajima, Y. Honda, O. Kitao, H. Nakai, T. Vreven, J.A. Montgomery Jr., J.E. Peralta, F. Ogliaro, M. Bearpark, J.J. Heyd, E. Brothers, K.N. Kudin, V.N. Staroverov, R. Kobayashi, J. Normand, K. Raghavachari, A. Rendell, J.C. Burant, S.S. Iyengar, J. Tomasi, M. Cossi, N. Rega, J.M. Millam, M. Klene, J.E. Knox, J.B. Cross, V. Bakken, C. Adamo, J. Jaramillo, R. Gomperts, R.E. Stratmann, O. Yazyev, A.J. Austin, R. Cammi, C. Pomelli, J.W. Ochterski, R.L. Martin, K. Morokuma, V.G. Zakrzewski, G.A. Voth, P. Salvador, J.J. Dannenberg, S. Dapprich, A.D. Daniels, O. Farkas, J.B. Foresman, J.V. Ortiz, J. Cioslowski, D.J. Fox, *Gaussian 09, Revision A.01*. Gaussian Inc., Wallingford (2009)
38. M. Evecen, H. Tanak, *Appl. Phys. A* **123**, 91 (2017)
39. E.S. Fatemi, M. Solimannejad, *Mater. Res. Express* **6**, 065016 (2019)
40. S. Ishikawa, T. Yamabe, *Appl. Phys. A* **123**, 119 (2017)
41. Z. Abdeveiszadeh, E. Shakerzadeh, S. Noorizadeh, *Heliyon* **5**, e01762 (2019)
42. S. Thakur, S.M. Borah, N.C. Adhikary, *Optik* **168**, 228 (2018)
43. S. Soleimani-Amiri, S. Badragheh, N. Asadbeigi, *J. Chin. Chem. Soc.* **66**, 866 (2019)
44. A.D. Becke, *Phys. Rev. A* **38**, 3098 (1988)
45. C. Lee, W. Yang, R.G. Parr, *Phys. Rev. B* **37**, 785 (1988)
46. Y. Yang, M.N. Weaver, K.M. Merz Jr., *J. Phys. Chem. A* **36**, 9843 (2009)
47. A.S. Rad, E. Abedini, *Appl. Surf. Sci.* **360**, 1041 (2016)
48. E. Lyngvi, F. Schoenebeck, *Tetrahedron* **69**, 5715 (2013)
49. D.L. Wang, H.L. Xu, Z.M. Su, D.Y. Hou, *Comput. Theor. Chem.* **978**, 166 (2011)
50. D. Wang, X. Wang, X. Gao, D. Hou, *Comput. Theor. Chem.* **989**, 33 (2012)
51. N.M. O'boyle, A.L. Tenderholt, K.M. Langner, *J. Comput. Chem.* **29**, 839 (2008)
52. T. Koopmans, *Physica* **1**, 104 (1933)
53. T. Lu, F. Chen, *J. Comput. Chem.* **33**, 580 (2011)
54. M.C.J.M. Vissenberg, M. Matters, *Phys. Rev. B* **57**, 12964 (1998)
55. H. Bässler, *Phys. Status Solidi B* **175**, 15 (2006)
56. B. Cordero, V. Gómez, A. E. Platero-Prats, M. Revés, J. Echeverría, E. Cremades, F. Barragán, S. Alvarez, *Dalton Trans.* 2832 (2008)
57. L. Pauling, *The Nature of the chemical bond* (Cornell University Press, Ithaca, 1960)
58. M. Koochi, S. Soleimani-Amiri, M. Shariati, *Struct. Chem.* **29**, 909 (2018)
59. S. Li, *Semiconductor physical electronics*, 2nd edn. (Springer, Berlin, 2006)
60. N. Otero, P. Karamanis, M. Mandado, *Phys. Chem. Chem. Phys.* **21**, 6274 (2019)

Publisher's Note Springer Nature remains neutral with regard to jurisdictional claims in published maps and institutional affiliations.